



Cite this: *Mater. Horiz.*, 2021, **8**, 1776

Received 11th November 2020,  
Accepted 18th March 2021

DOI: 10.1039/d0mh01826k  
rsc.li/materials-horizons

## Nanotherapeutics using all-natural materials. Effective treatment of wound biofilm infections using crosslinked nanoemulsions†

Cheng-Hsuan Li,‡<sup>a</sup> Ryan F. Landis,‡<sup>a</sup> Jessa Marie Makabenta,‡<sup>a</sup> Ahmed Nabawy,<sup>a</sup> Tiphaine Tronchet,<sup>a</sup> Danielle Archambault,<sup>b</sup> Yuanchang Liu,<sup>a</sup> Rui Huang,<sup>a</sup> Morgane Golan,<sup>b</sup> Wei Cui,<sup>b</sup> Jesse Mager,<sup>b</sup> Akash Gupta, <sup>a</sup> Suzannah Schmidt-Malan,<sup>c</sup> Robin Patel <sup>c</sup> and Vincent M. Rotello \*<sup>a</sup>

**Bacterial wound infections are a threat to public health. Although antibiotics currently provide front-line treatments for bacterial infections, the development of drug resistance coupled with the defenses provided through biofilm formation render these infections difficult, if not impossible, to cure. Antimicrobials from natural resources provide unique antimicrobial mechanisms and are generally recognized as safe and sustainable. Herein, an all-natural antimicrobial platform is reported. It is active against bacterial biofilms and accelerates healing of wound biofilm infections *in vivo*. This antimicrobial platform uses gelatin stabilized by photo-crosslinking using riboflavin (vitamin B<sub>2</sub>) as a photocatalyst, and carvacrol (the primary constituent of oregano oil) as the active antimicrobial. The engineered nanoemulsions demonstrate broad-spectrum antimicrobial activity towards drug-resistant bacterial biofilms and significantly expedite wound healing in an *in vivo* murine wound biofilm model. The antimicrobial activity, wound healing promotion, and biosafety of these nanoemulsions provide a readily translatable and sustainable strategy for managing wound infections.**

Antibiotics are the current treatment of choice for bacterial infections.<sup>1</sup> Unfortunately, bacteria are rapidly acquiring resistance against these agents through different mechanisms they have developed over billions of years to remove and/or deactivate toxins or evade their activities.<sup>2–4</sup> The ability of pathogenic bacteria,

### New concepts

Bacteria-associated infections are emerging threat to public health. Alternative treatment strategies to combat these infections are therefore an urgent priority. In this research, we show that readily available nature-derived components (gelatin, vitamin B<sub>2</sub>, essential oils) could be used to fabricate effective cross-linked nanoemulsions against refractory bacterial biofilms *in vitro* and *in vivo*. In contrast to most previous works, our approach only uses generally recognized as safe (GRAS) materials, further increasing safety and community acceptance. Moreover, all natural-derived therapeutics provide a sustainable path to manage diseases. Our study demonstrates the design of integrating all natural-derived materials for the treatment of bacterial biofilms. We envision that this design and concept contribute to the development of alternative antimicrobial strategies and therapeutics against other life-threatening diseases.

including *Pseudomonas aeruginosa* and *Staphylococcus aureus*, to form biofilms results in particularly problematic infections in wounds and on implanted devices.<sup>5,6</sup> The extracellular polymeric substance (EPS) matrix of biofilms has evolved as a barrier to some antibiotics and host immune responses. The slow growth and presence of persister cells in biofilms further foster resistance against traditional antibiotics.<sup>7</sup> Biofilms also impede the wound healing process, resulting in chronic wounds associated with increased morbidity, mortality, and decreased quality of life.<sup>8,9</sup> The lack of effective antibiofilm agents has led to an annual multibillion-dollar (US) burden to healthcare systems worldwide.<sup>10</sup>

Plant-derived essential oils provide a potential resource to combat bacterial biofilm-associated infections.<sup>11</sup> Essential oils are produced by plants as protection against infections by bacteria.<sup>12</sup> These oils have been extensively used in traditional medicine as antioxidant, anti-inflammatory and antibacterial agents, and their efficacy has been scientifically validated.<sup>13,14</sup> The additional benefits of using essential oils, including aroma,<sup>15</sup> safety,<sup>16</sup> and sustainability, have contributed to their increasing use in therapeutics. The low aqueous solubility of essential oils, however, limits their use in combating planktonic bacterial infections.<sup>17</sup> Moreover, these hydrophobic

<sup>a</sup> Department of Chemistry, University of Massachusetts Amherst,  
710 North Pleasant Street, Amherst, Massachusetts 01003, USA.

E-mail: rotello@chem.umass.edu

<sup>b</sup> Department of Veterinary and Animal Sciences, University of Massachusetts Amherst, 661 North Pleasant Street, Amherst, Massachusetts 01003, USA

<sup>c</sup> Division of Clinical Microbiology, Department of Laboratory Medicine and Pathology, Mayo Clinic, 200 First Street SW, Rochester, MN 55905, USA

† Electronic supplementary information (ESI) available: Detailed experimental methods, MBICs and MBBCs of gelatin nanoemulsions against bacterial biofilms, information of bacterial strains, stability and biodegradation of gelatin nanoemulsions determined by DLS, IR spectra of nanoemulsions, photographs of infected wounds, purulence scoring system, purulence scores of wounds, images of histological samples. See DOI: 10.1039/d0mh01826k

‡ These authors contributed equally to this work.

oils are not able to efficiently penetrate into the highly charged EPS of biofilms,<sup>18</sup> making them of limited use against biofilm-associated infections.

Synthetic nanoparticles and polymers provide a strategy for enhancing the activity of essential oil-based antimicrobials.<sup>19,20</sup> We set out to generate an all-natural platform that delivers active antimicrobials derived from essential oils for treatment of wound biofilms, with the potential for increased safety and community acceptance. In this platform, riboflavin (vitamin B<sub>2</sub>) is used to cross-link<sup>21,22</sup> gelatin that stabilizes nanodroplets of carvacrol, a key antimicrobial component of oregano oil. Our approach combines nature-derived ingredients to generate well-defined nanostructured-materials with size and stability required for potent antimicrobial and antibiofilm applications.<sup>23,24</sup> These nanoemulsions eradicated both Gram-positive and -negative

bacterial biofilms *in vitro*. Significantly, the nanoemulsion system was highly active *in vivo*, reducing bacterial loads in the wound site and enhancing the rate of wound healing in a murine wound biofilm model. Taken together, the described nanoemulsions used only bio-derived GRAS (generally regarded as safe) components to provide a safe, sustainable and effective treatment for wound biofilms.

The choice of oil for fabricating the nanoemulsions plays a critical role in therapeutic effects.<sup>25</sup> Oregano oil is among the most potent antimicrobial essential oils.<sup>19,26</sup> Carvacrol is the primary active component of oregano oil,<sup>19</sup> and was chosen to provide the GRAS benefits of oregano oil without the batch-to-batch variability observed with unpurified oils. Moreover, commercial gelatin was chosen as the scaffold for the oil-in-water nanoemulsion engineered to overcome the poor

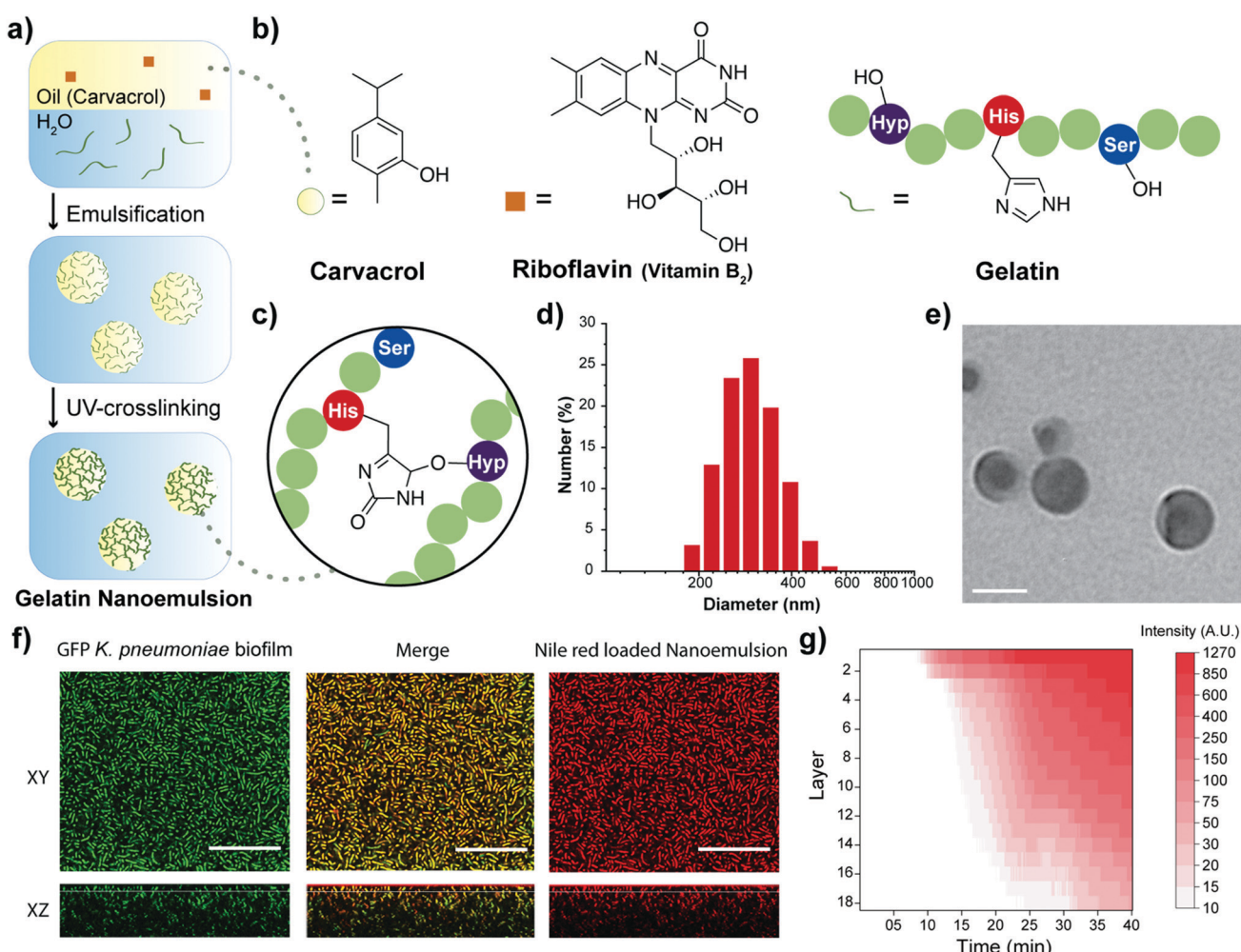


**Fig. 1** Fabrication and characterization of gelatin nanoemulsions. (a) Riboflavin (UV-cross-linking initiator) was dissolved in carvacrol. The oil mixture was then emulsified in an aqueous gelatin solution and cross-linked using long wavelength UV-A light (365 nm) to fabricate gelatin nanoemulsions. (b) Chemical structures of carvacrol, riboflavin, and the functional groups of gelatin participating in the cross-linking reaction. (c) Proposed cross-linked structure of gelatin nanoemulsions. (d) Dynamic light scattering histogram of nanoemulsions in phosphate buffered saline (150 mM). (e) Transmission electron microscopy images of nanoemulsions. Scale bar is 100 nm. (f) Confocal laser scanning microscopy images of green fluorescent protein-expressing *Klebsiella pneumoniae* (IDRL-11999) biofilm after 40 minutes treatment with Nile red-loaded nanoemulsions (XY top view, XZ side view). Scale bars are 50  $\mu$ m and the thickness of this biofilm is  $\sim$  37  $\mu$ m. (g) Spatial and time distribution of red fluorescence within the biofilm after the addition of Nile red-loaded nanoemulsions, indicating complete penetration after 35 min.

water solubility of carvacrol. Gelatin is naturally-derived, inherently biocompatible, biodegradable, non-cytotoxic, and has low antigenicity.<sup>27</sup> Structurally, gelatin is hydrophilic with hydrophobic domains, allowing it to encapsulate and stabilize hydrophobic oils, such as carvacrol, in aqueous condition.<sup>28</sup> The gelatin matrix was stabilized through a cross-linking technique used for therapeutic corneal collagen cross-linking.<sup>21</sup> This strategy employs riboflavin (vitamin B<sub>2</sub>) as a photo-initiator for cross-linking gelatin fibers. Nanoemulsions were fabricated by emulsifying a suspension of riboflavin in carvacrol into an aqueous suspension of gelatin (Fig. 1a), generating a transiently stable emulsion. This emulsion was then irradiated (365 nm) to activate the cross-linking process, resulting in stable nanoemulsions.

Dynamic light scattering (DLS), transmission electron microscopy (TEM) and attenuated total reflectance-Fourier transform infrared spectroscopy (ATR-FTIR) were used to characterize the nanoemulsions. DLS analysis showed that the hydrodynamic diameter of nanoemulsions is  $\sim 310$  nm with a narrow size distribution (polydispersity index = 0.017)

(Fig. 1d). These nanoemulsions are stable at room temperature for at least 30 days and are degraded in the presence of collagenase (Fig. S1, ESI<sup>†</sup>). TEM photographs revealed a spherical morphology of the nanoemulsions (Fig. 1e and Fig. S2, ESI<sup>†</sup>). The size observed in TEM ( $\sim 100$  nm) is smaller than observed by DLS, presumably due to partial collapse upon removal of carvacrol under vacuum during TEM. Finally, the chemical nature of the cross-linking was demonstrated by the emergence of a band at  $1033\text{ cm}^{-1}$  arising from aliphatic-aromatic ether formation, an additional aromatic ether signature at  $1242\text{ cm}^{-1}$ , and appearance of  $\text{sp}^3$  C-H stretches at  $2957\text{ cm}^{-1}$  (Fig. 1c and Fig. S3, ESI<sup>†</sup>).

Carvacrol and other hydrophobic materials fail to penetrate biofilms.<sup>18</sup> We hypothesized that the cationic charge of gelatin at the low pH<sup>29</sup> found in biofilms<sup>30</sup> would facilitate transport of nanoemulsions into biofilms. Confocal laser scanning microscopy (CLSM) was used to demonstrate effective and complete penetration of gelatin nanoemulsions into biofilms. Transport was tracked by loading the vehicle with the hydrophobic dye Nile red. Nanoemulsions were incubated with

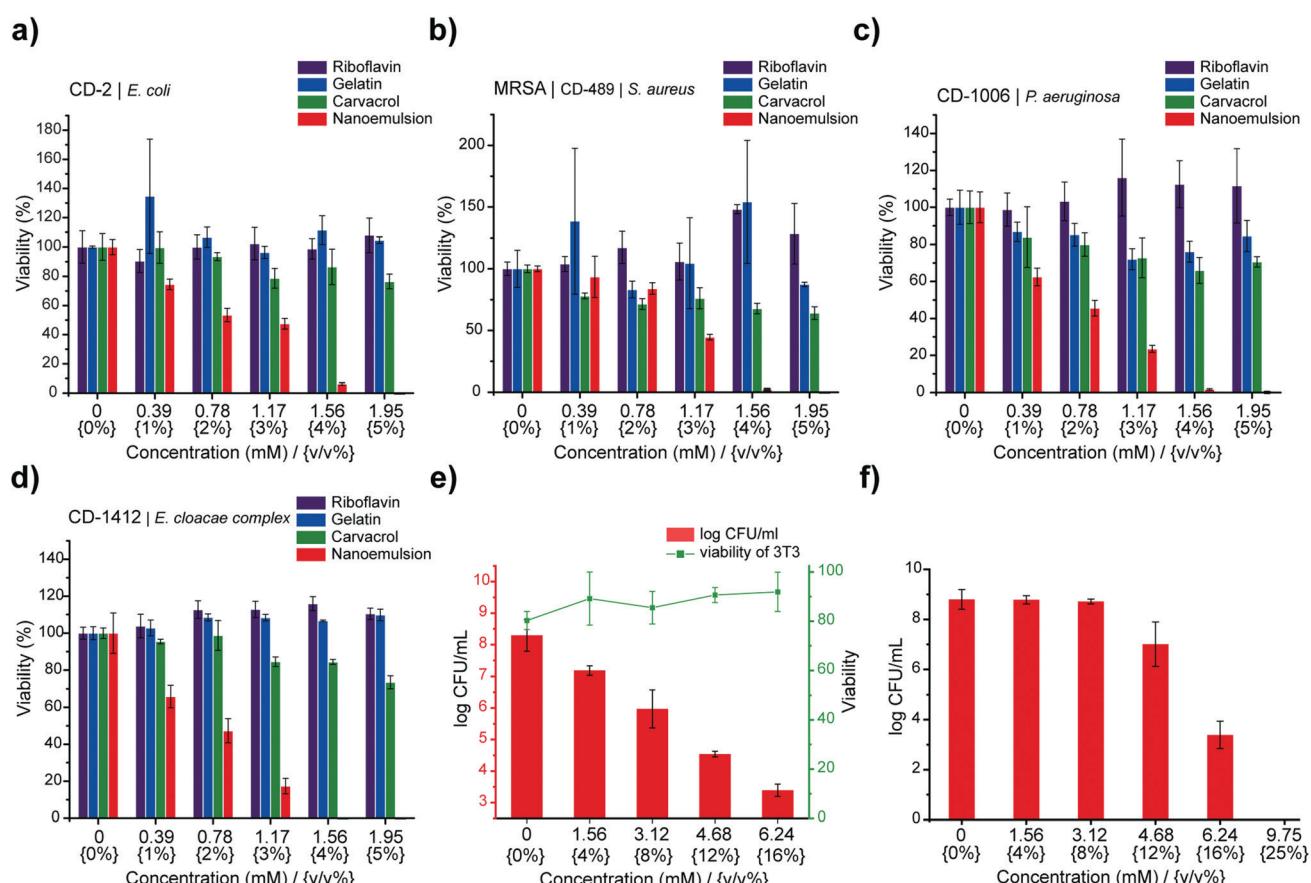


**Fig. 2** Gelatin nanoemulsions kill the bacteria within biofilms. Viability of (a) *Escherichia coli* CD-2, (b) methicillin-resistant *Staphylococcus aureus* CD-489, (c) *Pseudomonas aeruginosa* CD-1006, and (d) *Enterobacter cloacae* complex CD-1412 biofilms after 3 hours of treatment with riboflavin, gelatin, carvacrol, or nanoemulsions. (e) Viability of 3T3 fibroblast cells and *P. aeruginosa* biofilms in the co-culture model after 3 h treatment with nanoemulsions. Scatters and lines represent 3T3 fibroblast cell viability. Bars represent  $\log_{10}$  of colony forming units of bacteria in biofilms. (f) Gelatin nanoemulsions kill the biofilm bacteria in simulated wound conditions.  $\log_{10}$  colony forming units (CFU) of methicillin-resistant *Staphylococcus aureus* IDRL-6169 biofilms after 3 hours of treatment with gelatin nanoemulsions in simulated wound fluid. Data are presented as mean  $\pm$  standard deviation and represent three independent experiments.

4 day old biofilms of green fluorescent protein (GFP)-expressing *K. pneumoniae* IDRL-11999. As shown in Fig. 1f, gelatin nanoemulsions penetrated the biofilm matrix completely, as indicated by visualization of Nile red throughout the thickness of the biofilm, with colocalization of red and green signals. Time-dependent z-stack scanning demonstrated that complete penetration of nanoemulsions occurred within 40 minutes (Fig. 1g).

We next probed the mechanism of action of gelatin nanoemulsions. We hypothesized that gelatin nanoemulsions kill bacteria the same manner as carvacrol, namely through disrupting the cell membrane. We used propidium iodide (PI) staining to monitor the membrane permeability of bacteria.<sup>31</sup> Planktonic bacteria (*P. aeruginosa*, ATCC-27853) were treated with gelatin nanoemulsions or antibiotic ceftazidime (from  $0.125\times$  to  $4\times$  of their respective minimum inhibitory concentrations (MICs)) in the presence of PI. Gelatin nanoemulsion treatment immediately generated fluorescence inside bacteria, indicating that PI penetrated through the compromised cell membrane and bound to DNA (Fig. S4, ESI†). In contrast, bacteria treated with ceftazidime did not generate fluorescence, as ceftazidime does not directly act on the membrane. Significantly, studies have shown that therapeutics causing membrane disruption are unlikely to induce resistance,<sup>19</sup> as demonstrated in a recent effective treatment of burn infection models.<sup>32</sup>

After validating the biofilm penetration profile and the mechanism of action, we used alamarBlue assay to assess antimicrobial activity of nanoemulsions against biofilms of

four clinical bacterial isolates (*P. aeruginosa* CD-1006, methicillin-resistant *S. aureus* [MRSA] CD-489, *Escherichia coli* CD-2, and *Enterobacter cloacae* complex CD-1412). Treatment of these biofilms with nanoemulsions for 3 hours eliminated bacteria within the biofilms at 5% v/v (1.95 mM of carvacrol) (Fig. 2), with individual components of the nanoemulsions having minimal effect. Notably, treatment of bacteria with only gelatin (nutrient<sup>33</sup>) or riboflavin (nutrient/potential quorum sensing signal<sup>34</sup>) can enhance biofilm viability. We further quantified the minimum biofilm inhibitory concentrations (MBICs) and minimum biofilm eradication concentrations (MBECs) towards several clinical isolates (Table S1, ESI†), including *P. aeruginosa* (CD-1006, IDRL-11442, ATCC 27583) and MRSA (IDRL-6169) to represent bacterial species that are common constituents of wound biofilm infections.<sup>35</sup> All biofilms were suppressed or eradicated by nanoemulsions at concentrations ranging from 4% v/v (1.56 mM) to 8% v/v (3.12 mM). This activity was mirrored in more challenging dual-species biofilm models (MRSA/*P. aeruginosa* and MRSA/*E. coli*) (Table S1, ESI†).<sup>36</sup>

We next used an *in vitro* bacterial biofilm-mammalian cell coculture model to evaluate antimicrobial activity and biocompatibility of gelatin nanoemulsions. *P. aeruginosa* (ATCC-27853) was seeded on the monolayer of NIH 3T3-fibroblast cells for 6 hours to mimic biofilm infections on mammalian cells. Subsequently, the cocultures were treated with gelatin nanoemulsion for three hours. The viabilities of mammalian cells and bacteria were determined using LDH assay and colony counting, respectively. As shown in Fig. 2e, gelatin nanoemulsions

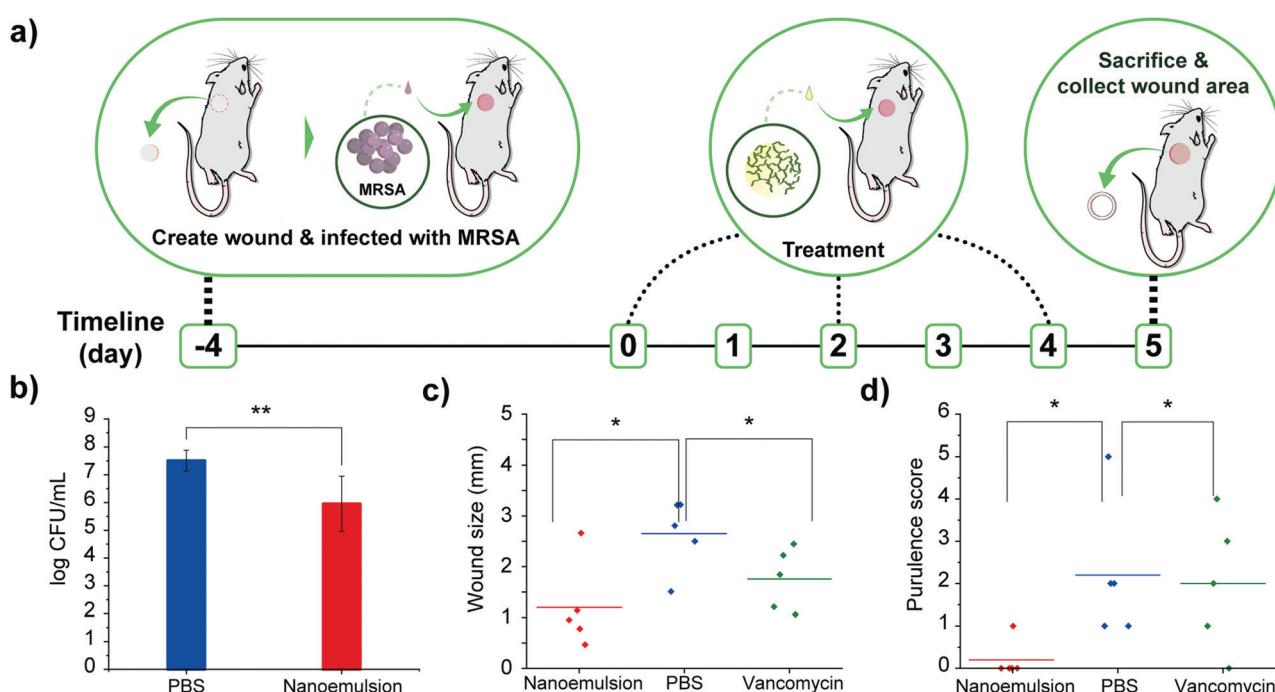


**Fig. 3** Gelatin nanoemulsions reduce bacterial load and expedite wound healing in a murine model *in vivo*. (a) Schematic overview of the murine biofilm-associated wound infection model. (b) Colony counts from the infected wounds treated with PBS and nanoemulsions. (c) Wound size at the day of sacrifice. (d) Purulence score at the day of sacrifice (\*, \*\* =  $P$  values  $<0.05$  or  $0.01$ , respectively).

effectively reduce bacterial colonies up to  $5 \log_{10}$  colony forming units (CFUs), while the toxicity toward 3T3 fibroblast cells remained negligible. Moreover, the activity of the nanoemulsions was determined using a simulated wound fluid (SWF) model, mimicking the interference/deactivation of antimicrobial activity by wound fluids.<sup>37</sup> In this experiment, 4 day old MRSA (IDRL-6169) biofilms were grown using tryptic soy broth (TSB)/SWF (1:1) solution. Gelatin nanoemulsions were serially diluted with SWF solution and added to the biofilms; three hours after, antimicrobial efficacy was determined using quantitative colony counting. Nanoemulsions were active against the biofilms in SWF, with 12% v/v (4.68 mM) and 16% v/v (6.24 mM) of nanoemulsions resulting in  $\sim 2$  and  $\sim 5 \log_{10}$  CFU reduction, respectively (Fig. 2f).

Encouraged by the *in vitro* efficacy of the nanoemulsions, their *in vivo* activity was evaluated using a murine wound biofilm model (Fig. 3a) designed to assess efficacy against established biofilms found in chronic wound infections.<sup>8,9</sup> In this model, MRSA IDRL-6169 biofilms were established in a wound created using a 5 mm skin puncture, and allowed to mature for 4 days. Mice were then separated into three groups: 100% v/v nanoemulsions (39 mM carvacrol), vancomycin (110 mg kg<sup>-1</sup>), and saline solution only. Treatments were administered every other day (topical application of nanoemulsions and PBS, and intraperitoneal injection of vancomycin) until the day of sacrifice. Photographs were taken daily, and

wound sizes and weights of the mice were monitored every day. The degree of purulence was also evaluated daily using a purulence reaction scoring system described in Fig. S5, ESI.<sup>†</sup>

Treatment with nanoemulsions significantly reduced bacterial load in the wound as compared with PBS controls, with  $\sim 1.5 \log_{10}$  unit reduction after administration of two treatments (Fig. 3b), a reduced degree of killing relative to *in vitro* studies owing to the much greater complexity of the *in vivo* environment. Significantly, vancomycin only had  $\sim 0.5 \log_{10}$  bacterial reduction (Fig. S6, ESI<sup>†</sup>). The antimicrobial effect of the nanoemulsions was mirrored by their enhanced wound healing. The group treated with nanoemulsions showed a greater reduction in wound size after treatment as compared to those treated with vancomycin or PBS (Fig. 3c), with the two control group wound beds still containing pus (Fig. S7–S9, ESI<sup>†</sup>). The wounds were likewise better healed: mice in the nanoemulsion group had a purulence score 0, with normally-appearing healed wound beds. In contrast, vancomycin and PBS groups had purulence scores  $\sim 2$ , indicating the presence of pus (Fig. 3d and Fig. S10, ESI<sup>†</sup>).

Histological analysis of the wound beds similarly indicated enhanced healing with the nanoemulsions. Hematoxylin and eosin staining (H&E staining) revealed regeneration of keratin and epithelial layers, and collagen matrix for the nanoemulsion group. In contrast, for the vancomycin and PBS groups,

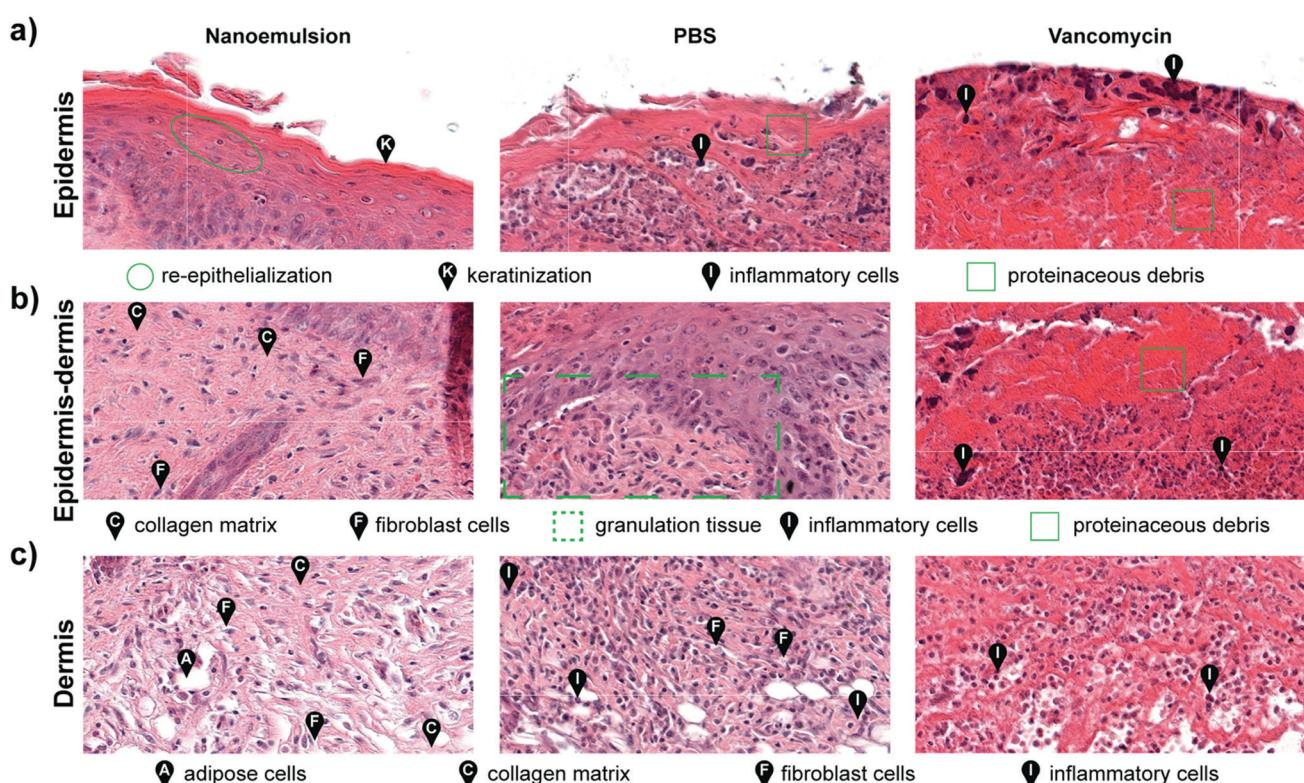


Fig. 4 Histological analysis of the tissues surrounding infected wounds show enhanced healing with nanoemulsions. (a) Epidermis samples showed regeneration of keratin and the epithelial layer with nanoemulsion treatment. In contrast, inflammatory cells and proteinaceous debris were observed with PBS and vancomycin treatments. (b) Substantial formation of collagen matrix at the epidermis-dermis junction was observed after nanoemulsion treatment, whereas immature epidermis and granulation were observed with PBS. Necrosis and cell debris were also detected in the vancomycin-treated sample. (c) The dermis was restored with nanoemulsion treatment, while inflammatory cells were still present in the PBS and vancomycin controls.

inflammatory cells were still abundantly found in the area, indicating that the wounds were in the early stages of the wound healing cascade (Fig. 4 and Fig. S11, ESI<sup>†</sup>). Notably, the healed skin had a normal appearing epidermis and dermis, suggesting that nanoemulsions do not alter morphology of the skin undergoing repair. The relative lack of inflammatory cells could also suggest an anti-inflammatory role for the nanoemulsions in wound healing.

## Conclusions

In summary, integration of nanostructured biomaterials with essential oil payloads provides effective treatment of challenging wound biofilms. Emulsification of oregano oil and gelatin followed by vitamin B<sub>2</sub> cross-linking provided stable nanoemulsions comprised solely of naturally-occurring components. These described nanoemulsions effectively penetrate into biofilms, and kill embedded Gram-positive and -negative bacteria effectively *in vitro*. This antibacterial effect is observed in an *in vivo* murine model, and translates into enhancement in wound healing both in terms of wound size and degree of purulence. Crucially, this platform is highly modular, providing a general platform for the delivery of a wide variety of oils and other payloads. Overall, integration of the inherent bactericidal activity of essential oils with materials properties provided by biomaterials presents a new path of treatment for wound biofilms, with potential for treating other life-threatening bacterial infections.

## Author contributions

R. F. L. and V. M. R. conceived, designed and fabricated gelatin nanoemulsions. R. F. L., C.-H. L., A. N. and R. H. characterized gelatin nanoemulsions. T. T., C.-H. L., J. M. M. and A. N. performed antimicrobial experiments *in vitro*. S. S. M. and R. P. helped design *in vivo* experiments and edited the manuscript. J. M. M., A. N., Y. L. and A. G. performed antimicrobial experiments *in vivo*. W. C. assisted in *in vivo* study. D. A. and J. M. carried out histological experiments and analysed data. C.-H. L., J. M. M. and V. M. R. wrote and revised the manuscript. All authors discussed the results and commented on the manuscript.

## Conflicts of interest

The authors declare no competing final interest.

## Acknowledgements

This research was supported by the NIH (AI134770). Clinical samples obtained from the Cooley Dickinson Hospital Microbiology Laboratory (Northampton, MA) were kindly provided by Dr Margaret Riley. The microscopy data was gathered in the Light Microscopy Facility and Nikon Center of Excellence at the

Institute for Applied Life Sciences, UMass Amherst with support from the Massachusetts Life Sciences Center.

## Notes and references

- 1 N. F. Col and R. W. O'Connor, *Rev. Infect. Dis.*, 1987, **9**, S232–S243.
- 2 J. M. A. Blair, M. A. Webber, A. J. Baylay, D. O. Ogbolu and L. J. V. Piddock, *Nat. Rev. Microbiol.*, 2015, **13**, 42–51.
- 3 R. Aminov, *Front. Microbiol.*, 2010, **1**, 134.
- 4 X. Liu, Z. Wang, X. Feng, E. Bai, Y. Xiong, X. Zhu, B. Shen, Y. Duan and Y. Huang, *Bioconjugate Chem.*, 2020, **31**, 1425–1437.
- 5 G. A. James, E. Swogger, R. Wolcott, E. deLancey Pulcini, P. Secor, J. Sestrich, J. W. Costerton and P. S. Stewart, *Wound Repair Regen.*, 2008, **16**, 37–44.
- 6 C. R. Arciola, D. Campoccia, P. Speziale, L. Montanaro and J. W. Costerton, *Biomaterials*, 2012, **33**, 5967–5982.
- 7 K. Lewis, *Curr. Top. Microbiol. Immunol.*, 2008, **322**, 107–131.
- 8 S. L. Percival, S. M. McCarty and B. Lipsky, *Adv. Wound Care*, 2014, **4**, 373–381.
- 9 C. Xu, O. U. Akakuru, X. Ma, J. Zheng, J. Zheng and A. Wu, *Bioconjugate Chem.*, 2020, **31**, 1708–1723.
- 10 K. Järbrink, G. Ni, H. Sönnnergren, A. Schmidtchen, C. Pang, R. Bajpai and J. Car, *Syst. Rev.*, 2017, **6**, 1–7.
- 11 M. Simões, R. N. Bennett and E. A. S. Rosa, *Nat. Prod. Rep.*, 2009, **26**, 746–757.
- 12 B. K. Tiwari, V. P. Valdramidis, C. P. O'Donnell, K. Muthukumarappan, P. Bourke and P. J. Cullen, *J. Agric. Food Chem.*, 2009, **57**, 5987–6000.
- 13 M. T. Baratta, H. J. D. Dorman, S. G. Deans, D. M. Biondi and G. Ruberto, *J. Essent. Oil Res.*, 1998, **10**, 618–627.
- 14 M. H. Farzaei, R. Bahrami-Soltani, Z. Abbasabadi and R. Rahimi, *J. Pharm. Pharmacol.*, 2015, **67**, 1467–1480.
- 15 M. Etman, M. Amin, A. H. Nada, M. Shams-Eldin and O. Salama, *Drug Discoveries Ther.*, 2011, **5**, 150–156.
- 16 G. Freire Rocha Caldas, A. V. Araújo, G. S. Albuquerque, J. D. C. Silva-Neto, J. H. Costa-Silva, I. R. A. De Menezes, A. C. L. Leite, J. G. M. Da Costa, A. G. Wanderley, G. F. R. Caldas, A. V. Araújo, G. S. Albuquerque, J. D. C. Silva-Neto, J. H. Costa-Silva, I. R. A. de Menezes, A. C. L. Leite, J. G. M. da Costa and A. Gonçalves-Wanderley, *Evidence-Based Complement. Altern. Med.*, 2013, **2013**, 856168.
- 17 C. Samperio, R. Boyer, W. N. Eigel, K. W. Holland, J. S. McKinney, S. F. O'Keefe, R. Smith and J. E. Marcy, *J. Agric. Food Chem.*, 2010, **58**, 12950–12956.
- 18 A. Iannitelli, R. Grande, A. Di Stefano, M. Di Giulio, P. Sozio, L. J. Bessa, S. Laserra, C. Paolini, F. Protasi and L. Cellini, *Int. J. Mol. Sci.*, 2011, **12**, 5039–5051.
- 19 R. F. Landis, C.-H. Li, A. Gupta, Y.-W. Lee, M. Yazdani, N. Ngernyuang, I. Altinbasak, S. Mansoor, M. A. S. Khichi, A. Sanyal and V. M. Rotello, *J. Am. Chem. Soc.*, 2018, **140**, 6176–6182.
- 20 A. Guarda, J. F. Rubilar, J. Miltz and M. J. Galotto, *Int. J. Food Microbiol.*, 2011, **146**, 144–150.

21 G. Wollensak, E. Spoerl and T. Seiler, *Am. J. Ophthalmol.*, 2003, **135**, 620–627.

22 J. Ribes, N. Beztsinna, R. Bailly, S. Castano, E. Rascol, N. Taib-Maamar, E. Badarau and I. Bestel, *Bioconjugate Chem.*, 2021, **32**, 553–562.

23 J. M. V. Makabenta, A. Nabawy, C.-H. Li, S. Schmidt-Malan, R. Patel and V. M. Rotello, *Nat. Rev. Microbiol.*, 2021, **19**, 23–36.

24 Y. Liu, L. Shi, L. Su, H. C. Van der Mei, P. C. Jutte, Y. Ren and H. J. Busscher, *Chem. Soc. Rev.*, 2019, **48**, 428–446.

25 N. Terjung, M. Löffler, M. Gibis, J. Hinrichs and J. Weiss, *Food Funct.*, 2012, **3**, 290–301.

26 A. Nostro, A. R. Blanco, M. A. Cannatelli, V. Enea, G. Flamini, I. Morelli, A. S. Roccaro and V. Alonzo, *FEMS Microbiol. Lett.*, 2004, **230**, 191–195.

27 A. O. Elzoghby, *J. Controlled Release*, 2013, **172**, 1075–1091.

28 E. Dickinson, *Food Hydrocolloids*, 2009, **23**, 1473–1482.

29 B. Gaihre, M. S. Khil, D. R. Lee and H. Y. Kim, *Int. J. Pharm.*, 2009, **365**, 180–189.

30 J. M. Vroom, K. J. De Grauw, H. C. Gerritsen, D. J. Bradshaw, P. D. Marsh, G. K. Watson, J. J. Birmingham and C. Allison, *Appl. Environ. Microbiol.*, 1999, **65**, 3502–3511.

31 D. J. Arndt-Jovin and T. M. Jovin, in *Fluorescence Microscopy of Living Cells in Culture Part B. Quantitative Fluorescence Microscopy—Imaging and Spectroscopy*, ed. D. L. Taylor and Y.-L. Wang, Academic Press, 1989, vol. 30, pp. 417–448.

32 M. Lu, S. Wang, T. Wang, S. Hu, B. Bhayana, M. Ishii, Y. Kong, Y. Cai, T. Dai, W. Cui and M. X. Wu, *Sci. Transl. Med.*, 2021, **13**, eaba3571.

33 S. A. Koser, B. D. Chinn and F. Saunders, *J. Bacteriol.*, 1938, **36**, 57–65.

34 S. Rajamani, W. D. Bauer, J. B. Robinson, J. M. Farrow, E. C. Pesci, M. Teplitski, M. Gao, R. T. Sayre and D. A. Phillips, *Mol. Plant-Microbe Interact.*, 2008, **21**, 1184–1192.

35 R. Serra, R. Grande, L. Butrico, A. Rossi, U. F. Settimio, B. Caroleo, B. Amato, L. Gallelli and S. de Franciscis, *Expert Rev. Anti-Infect. Ther.*, 2015, **13**, 605–613.

36 S. DeLeon, A. Clinton, H. Fowler, J. Everett, A. R. Horswill and K. P. Rumbaugh, *Infect. Immun.*, 2014, **82**, 4718–4728.

37 W. A. Craig and P. G. Welling, *Clin. Pharmacokinet.*, 1977, **2**, 252–268.